

# Theoretical analysis of lens array for uniform irradiation on target in multimode fiber lasers

Jian Lin (林健), Lixin Xu (许立新)\*, Shengbo Wang (王声波),  
and Haixiao Han (韩海啸)

Anhui Key Laboratory of Optoelectronic Science and Technology, Department of Optics and  
Optical Engineering, University of Science and Technology of China, Hefei 230026, China

\*Corresponding author: xulixin@ustc.edu.cn

Received April 14, 2014; accepted July 16, 2014; posted online September 28, 2014

We propose and demonstrate a scheme to smooth and shape the on-target patterns in multimode fiber lasers, which includes expanding–collimating system and lens array (LA). A smooth pattern with flat-top and sharp-edge profiles can be obtained with the irradiation nonuniformity decreasing significantly. We analyze the effects of the parameters such as defocus distance, the tilt angles, the number of the incident fiber lasers, and the diffraction-weakened LA on the uniformity irradiation of target by numerical simulations.

OCIS codes: 140.3298, 140.3300, 140.3510, 260.1960.

doi: 10.3788/COL201412.101402.

Fiber lasers have been intensively studied in recent years. When compared with other kinds of lasers, fiber lasers have many advantages such as high conversion efficiency, convenient heat management, and excellent beam quality, which are widely used in many fields. However, the output power of single-fiber laser is limited due to the nonlinear effect, heat damage, and the brightness of the pump source. Beam combining of laser array is an effective way to significantly improve the output power and brightness<sup>[1–3]</sup>. Labaune *et al.*<sup>[4]</sup> proposed a new concept of inertial confinement fusion (ICF) based on fiber application network, to combine a large number of fiber amplifiers as ICF driver. Adopting the direct-drive shock ignition, the uniform on-target irradiation is one of the key requirements<sup>[5–7]</sup>. Also, in many other applications the transformation of the intensity distribution of laser beam into a top hat is required. In laser display, uneven imaging problem exists, and the uneven brightness on the screen is a serious impediment to the rapid development of laser display technology.

A number of smoothing methods have been developed, such as spatial smoothing, temporal smoothing, and polarization smoothing. Among spatial smoothing, there are distributed phase plate (DPP)<sup>[8]</sup>, continuous phase plate (CPP)<sup>[9,10]</sup>, lens array (LA)<sup>[11–13]</sup>, and so on. DPP and CPP can achieve high diffraction efficiency and the focal spot distribution profile can be controlled according to the demand, but its scattering losses cannot be ignored and is sensitive to near-field distortion of the incident beam. There are several research studies on using special compound mode of laser beams to get flat spot on target plane and indeed obtain satisfactory results. But they need complex designs of compound mode of laser beams and have strong limits to the modes of light field. LA is insensitive to near-field distortion and it seems to be an effective tool for uniform irradiation in multimode fiber lasers.

Here we develop a smoothing scheme employing expanding–collimating system and LA to overlay the multiple fiber lasers. From the simulation results, we can greatly reduce the nonuniformity on target by setting a suitable defocus distance, increasing the number of fibers, adding a random angle within a certain range to each fiber, and adopting soft-edge LA. This scheme offers a useful method to smooth and shape the target patterns.

The configuration of our scheme with a LA is shown in Fig. 1. The fiber lasers are arranged equidistantly. In order to get higher power, we employ multimode fibers. The lenses  $L_1$  and  $L_2$  form the expanding–collimating system. Suppose the output laser field of the  $n$ th fiber is  $E_{0n}(x_0, y_0)$ , when it passes concave lens  $L_1$ , the divergence of the beam will become larger, then passes convex lens  $L_2$ , the beam will be expanded and collimated. The incident light field before LA is  $E_{1n}(x_1, y_1)$ , and it is approximately parallel light.

Suppose LA has  $M \times M$  lens elements and all of them are square shaped with the same aperture  $d$  and the focal length  $F_c$ . Each incident beam is cut into

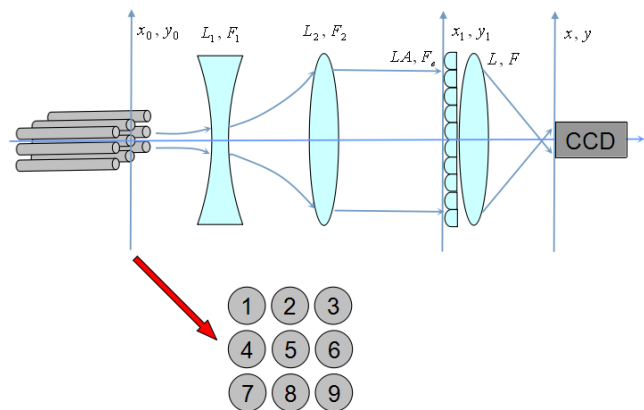


Fig. 1. Configuration of the optical system with LA.

many beamlets by LA and then focused by the principal focusing lens  $L$  to form a pattern, and at last each pattern from different fibers are incoherently overlaid on the target. The focal length and aperture of  $L$  are denoted as  $F$  and  $D$ , respectively, and  $D = Md$ . When the target is placed at the focus of  $L$ , the pattern size  $a$  can be given by

$$a = \frac{d \cdot F}{F_e}. \quad (1)$$

To further improve the irradiation uniformity of the pattern, the target is usually placed at the defocus plane rather than at the focal plane of the principal focusing lens, and the moving distance is  $\Delta z$ , we define  $\Delta z$  is negative before the focus and positive after the focus. The complex transmittance of LA is given by

$$T_1(x, y) = \sum_{m_1, m_2} \delta(x - m_1 d, y - m_2 d) \cdot \exp \left\{ -i \frac{k}{2F_e} [(x - m_1 d)^2 + (y - m_2 d)^2] \right\}, \quad (2)$$

where  $k$  is the wave number of incident laser, and  $-\frac{M-1}{2} \leq m_1, m_2 \leq \frac{M-1}{2}$ . The center coordinate of the element located in row  $m_1$  and column  $m_2$  is  $(m_1 d, m_2 d)$ .  $\delta(x_1, y_1)$  is the pupil function defined by

$$\delta(x_1, y_1) = \begin{cases} 1, & \text{inside the lens aperture} \\ 0, & \text{otherwise} \end{cases}. \quad (3)$$

The complex transmittance of the principal focal lens  $L$  is

$$T_2(x, y) = \exp \left[ -i \frac{k}{2F} (x^2 + y^2) \right]. \quad (4)$$

According to the Fresnel diffraction formula<sup>[13]</sup>, we can get the light field from the  $n$ th fiber on the target:

$$E_n(x, y) = \frac{\exp[ik(F + \Delta z)]}{i\lambda(F + \Delta z)} \iint E_{1n}(x_1, y_1) \cdot T_1(x_1, y_1) \cdot T_2(x, y) \cdot \exp \left\{ \frac{ik}{2(F + \Delta z)} [(x - x_1)^2 + (y - y_1)^2] \right\} dx_1 dy_1. \quad (5)$$

At last all patterns from different fibers incoherently superpose on the target, so the final light field is

$$I(x, y) = \sum_{n=1}^N |E_n(x, y)|^2. \quad (6)$$

If the number of the lens elements of LA is very large, for the interference speckle, the probability density function of light intensity distribution satisfies the decreasing exponential distribution<sup>[14]</sup>:

$$P(I) = \frac{1}{\bar{I}} \exp \left( -\frac{I}{\bar{I}} \right), \quad (7)$$

where  $\bar{I}$  is the average intensity. From Eq. (7), we can see that the probability density of zero intensity is the largest, so it has a high-intensity contrast.

Uniformity is defined as

$$\text{RMS} = \frac{\sqrt{\langle (I - \bar{I})^2 \rangle}}{\bar{I}}. \quad (8)$$

For the speckle caused by coherent light passing through LA, from Eq. (7),  $\bar{I}^2 = 2I$ , substituting it into Eq. (8), we obtain the uniformity of the speckle being 1, which reaches the maximum.

When multiple speckles whose intensities distribute irrelevantly superpose independently on the target, probability density of light intensity distribution is no longer the same as the single speckle. If each speckle has the same statistical property and the same average intensity, the probability density of light intensity distribution by superposition of the interference speckle can be written as

$$P_N(I) = \frac{N^N \cdot I^{N-1}}{(N-1)! \bar{I}^N} \exp \left( -\frac{NI}{\bar{I}} \right), \quad (9)$$

where  $\bar{I}$  is the average intensity of the speckles after superposition. Now, the probability density of zero intensity greatly reduces, and the intensity contrast decreases at the same time.

The relationship between the probability density of light intensity distribution and the increasing number of the independent speckles superposed by Eq. (9) is shown in Fig. 2. From Fig. 2, we can see that with the increase in number  $N$ , the probability densities of light and dark intensities are reduced, the peak of the probability density is toward the average intensity, and lastly the intensity distributes around the average intensity within a narrow range, so the nonuniformity decreases.

Substituting Eq. (9) into Eq. (8), we obtain the uniformity of the intensity superposed by  $N$  speckles:

$$\text{RMS} = \frac{1}{\sqrt{N}}, \quad (10)$$

where the uniformity is inversely proportional to  $\sqrt{N}$ .

There are two methods to increase the number of the independent speckles: 1) let multiple independent and unrelated spots (staggered) superpose on the target at

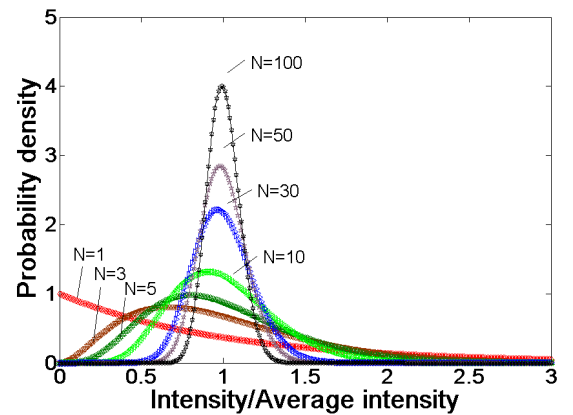


Fig. 2. Probability density of light intensity distribution by superposition of the interference speckle.

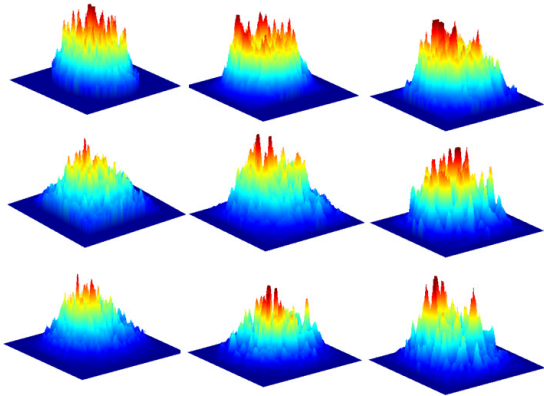


Fig. 3. Incident light field before LA of each fiber.

the same time, so the spots get instant smoothing and 2) make the speckle vary rapidly in a very short time, multiple independent speckles superpose from the effect of cumulative time (such as SSD technology)<sup>[15,16]</sup>, so the spot gets smoothed.

We use multiple incident fibers, and purport to make each spot from different fiber staggered, so the uniformity of the spot superposed will be reduced on the target, and it is a method of instant smoothing.

Based on the principles described above, the intensity distribution of the on-target pattern is simulated. The  $3 \times 3$  incident fibers are multimode fiber, and the wavelength of the incident beams is 1053 nm. We use experimental data for the incident light field before LA (the real output light field distribution of multimode fibers). Each beam is approximately parallel light and with about 40 mm aperture, but the light field distribution is different from each other (see Fig. 3).

The LA is composed of  $10 \times 10$  square elements, each with a 20 mm width and a 5000 mm focal length. The focal length of the principal focusing lens is 500 mm with a 200 mm aperture. From Eq. (1), the target spot size is about  $a = 2$  mm, and the interference speckle spacing is  $\Delta = \lambda F/d = 25$  mm.

We define two parameters to characterize the laser irradiation on the target. One is the root mean square (RMS) illumination nonuniformity defined as

$$\text{RMS} = \left[ \frac{\langle (I(x,y) - \bar{I})^2 \rangle}{\bar{I}^2} \right]^{1/2}, \quad (11)$$

and the other is power in bucket (PIB) defined by

$$\text{PIB} = \frac{\text{energy of the flat top of the spot}}{\text{total energy of the spot}}, \quad (12)$$

where  $I(x, y)$  is the intensity at any point within the flat top of the spot, and  $\bar{I}$  is the average intensity of the flat top. The angle brackets imply an ensemble average. RMS shows how flat the top pattern profile is and PIB provides the energy efficiency of the flat top. Our aim is to get a small RMS and a large PIB.

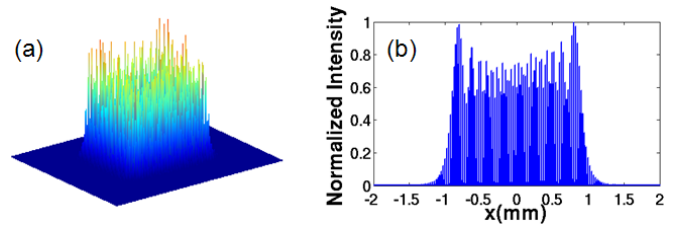


Fig. 4. (a) 3D intensity distribution of the target pattern on the focal plane and (b) distribution across the center of the pattern along the  $x$ -direction.

When the LA system is irradiated by an incident beam from one fiber, the intensity distribution in the focal plane is shown in Fig. 4. This is a quasi-near-field diffraction pattern with a high-intensity structure. When the beam passes through a lens element, the Fresnel diffraction arises and the intensity stripes are caused by interference between beamlets. If the target is placed at the defocus (see Fig. 5), where the moving distance  $\Delta z = 0.9$  mm, the sharp edge of the spot is improved, and the modulation depth of the interference stripes is reduced. The power spectral density (PSD) curves are shown in Fig. 6. When we compare focus with defocus, we find that mid-frequency component significantly decreases at the defocus, but high-frequency modulation remains, and RMS reduces to 71.45%.

We increase the number of the fibers, but the multiple fibers are absolutely collimated without any stagger angle with each other. We consider one fiber, two fibers, four fibers, and nine fibers, respectively, when the moving distance  $\Delta z$  is 0.9 mm. In Fig. 7, when the number of fibers ( $N$ ) varies from 1 to 2, the modulation depth of the intensity decreases obviously and the RMS reduces too (as also shown in Fig. 8). But when  $N$  increases further, the RMS changes slowly, especially when  $N$  varies from 4 to 9, the RMS does not decrease. By comparing the PSD curves with different values of  $N$  (Fig. 9), it can be seen that the low-frequency and mid-frequency (spatial period greater than  $40 \mu\text{m}$ ) components have been smoothed out to some extent, but the effect of smoothing of high-frequency (spatial period less than  $40 \mu\text{m}$ ) modulation is not significant, and increasing the value of  $N$  further has little meaning for smoothing the spot. The reason is that

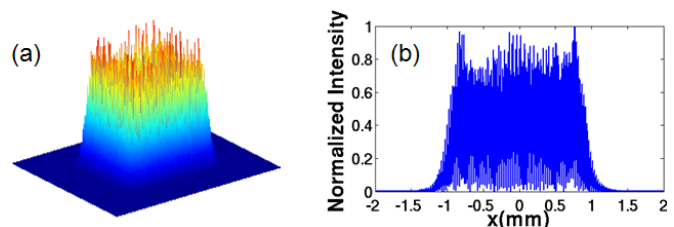


Fig. 5. (a) 3D intensity distribution of the target pattern with the target moving distance  $\Delta z = 0.9$  mm and (b) distribution across the center of the pattern along the  $x$ -direction.

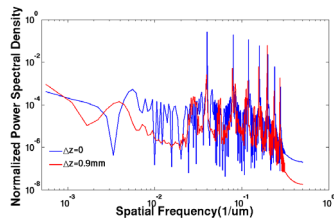


Fig. 6. PSD curves when  $\Delta z = 0$  and 0.9 mm.

all fibers are absolutely collimated without no stagger angle with each other, so the spots produced by each fiber on the target are coincident without staggering a little distance, and the interference fringes cannot be wiped out by peak to valley, at last only the contour can be smoothed.

In order to make each spot generated by different fibers stagger a little distance on the target, we consider adding a little random angle within a certain range to each fiber. The  $\Delta\theta_x$  ( $\sim 10^{-4}$ ) deflection angle of the beam before LA in the  $x$ -direction will lead to an  $F \cdot \Delta\theta_x$  shift of the spot on the target in corresponding direction, so the number of the independent speckles increases, the RMS reduces meantime.

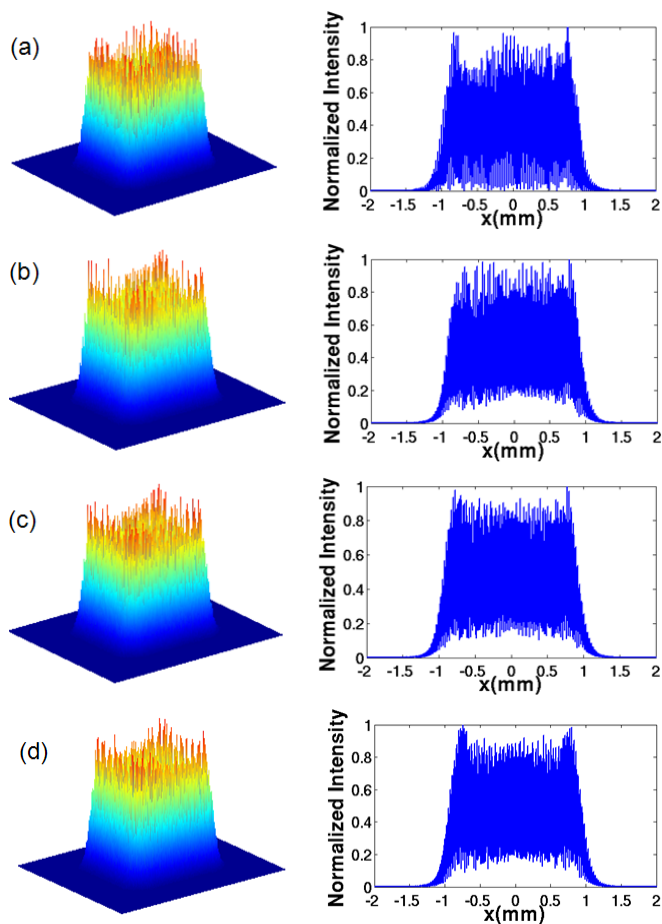


Fig. 7. Intensity distribution of the target pattern ( $\Delta z = 0.9$  mm): (a)  $N = 1$ , (b)  $N = 2$ , (c)  $N = 4$ , and (d)  $N = 9$ .

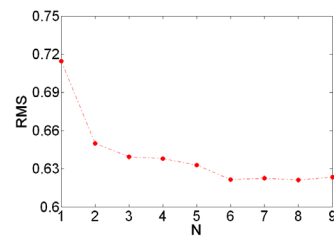


Fig. 8. Nonuniformity versus the number of fibers when the multiple fibers are absolutely collimated with each other.

From the light field distributions on the target with different  $N$  ( $\Delta z = 0.9$  mm) in Fig. 10, we can see that with the increase in  $N$ , the modulation depth of the light intensity decreases, and the zero intensity never appears. We have observed the individual light fields from different fiber lasers and find the different light spots stagger a little on target and some peaks in one spot correspond to some valleys in other spots. So when they incoherently overlay on target, the interference fringes can be partially wiped out. Figure 11 shows how the nonuniformity RMS varies versus  $\sqrt{N}$ . The RMS reduces rapidly approximately by  $1/\sqrt{N}$ , which is consistent with our statistical interpretations of the speckles. The staggered spots act as multiple independent and unrelated spots, and superpose independently on the target, so the probability density of light intensity distribution by superposition of the interference speckle satisfies Eq. (9) and the corresponding RMS reduces. According to the PSD curves in Fig. 12, it can be seen that with the increase in  $N$ , the modulation of the components whose spatial period is more than  $50 \mu\text{m}$  greatly reduces, and the modulation of the components with less than  $50 \mu\text{m}$  spatial period is smoothed to some extent too.

In the above simulations, the distance between different beams before LA is 20 mm. We have changed the distance and also tried to suppose different laser beams, for example, when  $N = 4$ , we suppose different combinations of four beams, such as 1, 2, 3, and 4 or 5, 6, 7, 8, and so on, and at last we find that the RMS changes a little in different conditions. The RMS mainly depends on the number of fiber lasers. So our configuration provides a compact and highly tolerant method for uniform irradiation.

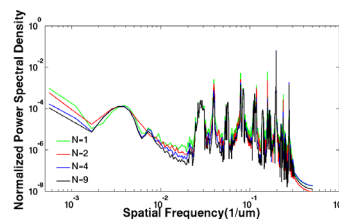


Fig. 9. PSD curves with different  $N$  when the multiple fibers are absolutely collimated with each other.

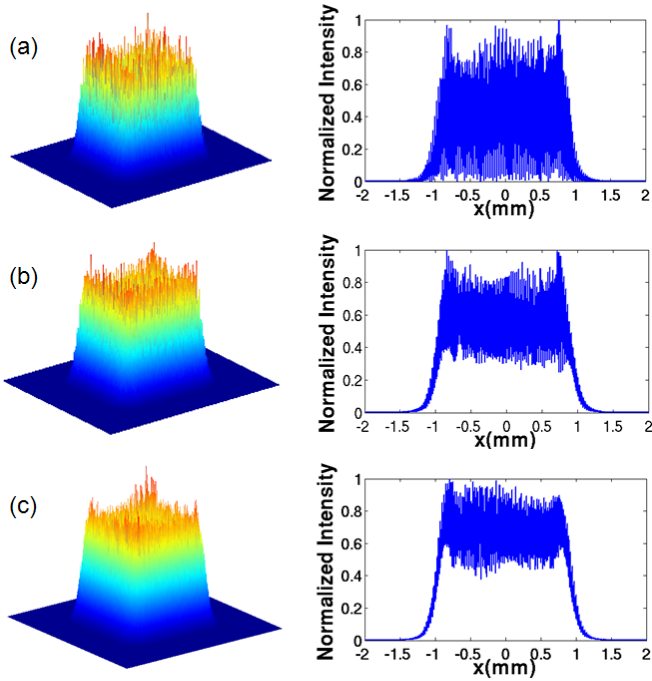


Fig. 10. Intensity distribution of the target pattern ( $\Delta z = 0.9$  mm): (a)  $N = 1$ , (b)  $N = 4$ , and (c)  $N = 9$  when each fiber is combined with a random little angle.

In ICF, the fine stripes within the focal spot can be eliminated by the effect of the plasma thermal conduction<sup>[17]</sup>. Laser intensity fluctuation of the range of  $20 \mu\text{m}$  seems not to bring about a severe laser imprinting effect in the laser produced shock experiments. We use spatial mean filtering technique within the range of  $20 \mu\text{m}$  to remove the high-frequency component of the spatial light intensity distribution in the numerical simulations. The result is shown in Fig. 13,  $\text{RMS} = 6.14\%$  and  $\text{PIB} = 82.22\%$ .

The simulation results have been proved in our experiment. The finite resolution of detecting CCD just plays the role of spatial filter which is approximately equivalent to the action of the heat conduction. A spot with  $\text{RMS}$  less than  $5\%$  has been obtained and is shown in Fig. 14. The related detailed results will be discussed in another paper soon.

According to Sommerfeld boundary diffraction theory, when a beam passes through an aperture, the light field on target is superimposed by the diffraction

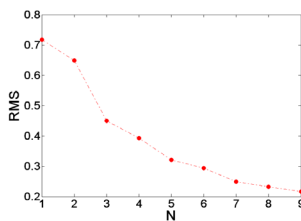


Fig. 11. Nonuniformity versus the number of fibers when each fiber is combined with a random little angle.

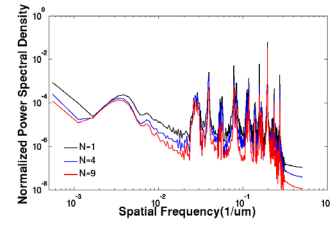


Fig. 12. PSD curves with different  $N$  when each fiber is combined with a random little angle.

wavelets generated by the hard-edge of LA and the directly transmitted light. Therefore, we consider using the edge of the refractive index gradient LA elements to eliminate edge diffraction effects<sup>[18]</sup>. The complex transmittance function of each LA element is

$$T_1(x_1, y_1) = \exp \left[ -\left( \frac{x_1}{d/2} \right)^{np} - \left( \frac{y_1}{d/2} \right)^{np} \right] \cdot \exp \left[ -i \frac{k}{2F_e} (x_1^2 + y_1^2) \right]. \quad (13)$$

And the intensity distribution of the target pattern is as shown in Fig. 15. Choosing an opposite  $np$ , the large-scale fluctuations caused by diffraction of the focal spot have been weakened, especially the sharp edge nearly disappears, but the modulation depth increases at the same time. If thermal conduction smoothing is considered,  $\text{RMS} = 4.31\%$  and  $\text{PIB} = 80.80\%$ .

In conclusion, we develop a scheme with an expanding-collimating system and LA in order to smooth and shape the on-target laser patterns in multimode fiber lasers. By setting a suitable defocus distance, increasing the number of fibers, adding a random angle within a certain range to each fiber, and using

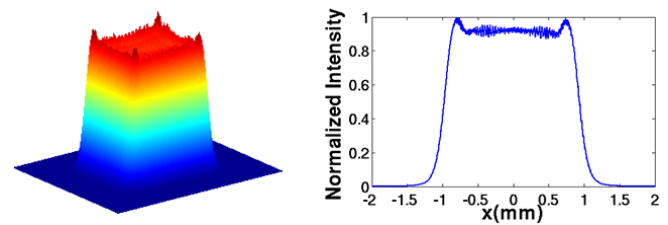


Fig. 13. Intensity distribution of the target pattern ( $\Delta z = 0.9$  mm) when thermal conduction smoothing is considered.

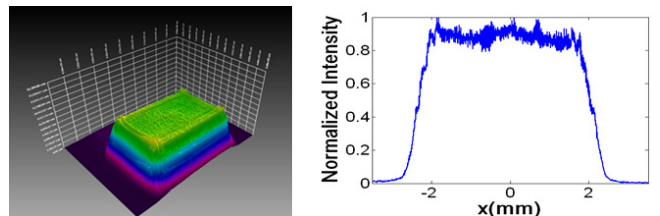


Fig. 14. Intensity distribution of the target pattern in experiment.

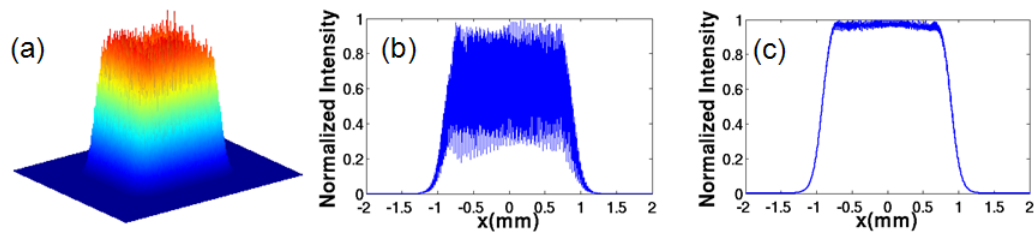


Fig. 15. Intensity distribution of the target pattern ( $\Delta z = 0.9$  mm,  $np = 20$ ): (a) 3D intensity distribution with a sharp-edged LA, (b) 1D intensity distribution with a diffraction-weakened LA, and (c) 1D intensity distribution with a diffraction-weakened LA when thermal conduction smoothing is considered.

diffraction-weakened LAs, we obtain the spot on the target with greatly decreasing RMS. If thermal conduction smoothing is considered, the RMS can be reduced to about 4% with PIB above 80%. Increasing the number of the laser fibers provides further improvement of the final laser intensity uniformity. Our work provides a beneficial reference for beam smoothing.

This work was supported by the National Natural Science Foundation of China under Grant No. 11374285.

## References

1. T. Y. Fan, IEEE J. Sel. Top. Quant. Electron. **11**, 567 (2005).
2. C. Geng, B. Zhao, E. Zhang, W. Luo, Y. Tan, Y. Zhu, H. Yang, J. Mu, X. Li, K. Duan, and W. Zhao, IEEE Photon. Technol. Lett. **25**, 1286 (2013).
3. P. Ma, P. Zhou, Y. Ma, R. Su, and Z. Liu, Chin. Opt. Lett. **10**, 081404 (2012).
4. C. Labaune, D. Hulin, A. Galvanauskas, and G. A. Mourou, Opt. Commun. **281**, 4075 (2008).
5. T. Xu, L. Xu, A. Wang, C. Gu, S. Wang, J. Liu, and A. Wei, Phys. Plasmas **20**, 122702 (2013).
6. M. Temporal, B. Canaud, W. J. Garbett, and R. Ramis, High Power Laser Sci. Eng. **2**, e8 (2014).
7. M. Temporal, B. Canaud, W. J. Garbett, and R. Ramis, Phys. Plasmas **21**, 012710 (2014).
8. Y. Lin, T. J. Kessler, and G. N. Lawrence, Opt. Lett. **20**, 764 (1995).
9. Y. Lin, T. J. Kessler, and G. N. Lawrence, Opt. Lett. **21**, 1703 (1996).
10. X. Jiang, J. Li, R. Wu, Z. Zhu, S. Zhou, and Z. Lin, J. Opt. Soc. Am. A **30**, 2162 (2013).
11. X. Deng, X. Liang, Z. Chen, W. Yu, and R. Ma, Appl. Opt. **25**, 377 (1986).
12. W. Cheng, X. Zhang, J. Su, S. Zhao, P. Li, J. Dong, and L. Zhou, J. Opt. A **11**, 15709 (2009).
13. X. Jiang, J. Li, H. Li, Y. Li, and Z. Lin, Appl. Opt. **50**, 5213 (2011).
14. J. C. Dainty, *Laser Speckles and Related Phenomena* (Springer, 1975).
15. S. Skupsky and R. S. Craxton, Phys. Plasmas **6**, 2157 (1999).
16. Y. Jiang, S. Zhou, R. Wu, J. Li, X. Li, and Z. Lin, Chin. Opt. Lett. **11**, 081404 (2013).
17. V. N. Goncharov, S. Skupsky, T. R. Boehly, J. P. Knauer, P. McKenty, V. A. Smalyuk, R. P. J. Town, O. V. Gotchev, R. Betti, and D. D. Meyerhofer, Phys. Plasmas **7**, 2062 (2000).
18. Y. Qiu, L. Qian, H. Huang, D. Fan, and X. Deng, Chin. J. Laser **22**, 27 (1995).